

DUPLICATE ALSO



# Forecasting Research

**Forecasting Research Division  
Scientific Paper No.19**

## **A Semi-Geostrophic Ocean Model with Outcropping**

by

**Paul Cloke  
and**

**M.J.P. Cullen**

**August 25, 1993**

**Meteorological Office  
London Road  
Bracknell  
Berkshire  
RG12 2SZ  
United Kingdom**

ORGS UKMO F

**National Meteorological Library**  
FitzRoy Road, Exeter, Devon. EX1 3PB

**Forecasting Research Division  
Scientific Paper No.19**

**A Semi-Geostrophic Ocean Model  
with Outcropping**

by

**Paul Cloke  
and**

**M.J.P. Cullen**

**August 25, 1993**

Forecasting Research Division

Scientific Paper No.19

A Semi-Geostrophic Ocean Model  
with Outcropping

by

Paul Cloke

and

M.J.P. Cullen

August 25, 1993

Forecasting Research Division  
Meteorological Office  
London Road  
Bracknell  
Berkshire RG12 2SZ  
ENGLAND

N.B This paper has not been published. Permission to quote from it must be obtained from the Head of Numerical Modelling Research at the Meteorological Office

## Abstract

A numerical model is presented. The model represents a single shallow water layer of constant density. The model is based upon the semi-geostrophic (SG) equations sometimes called the geostrophic momentum approximation (GM), an equation set which does not support gravity waves. These equations are intermediate in accuracy between the quasi-geostrophic (QG) equations and the shallow water equations. In contrast to the more common QG equations the SG set is valid for large layer thickness perturbations. The SG set also has the advantage over many other balanced sets in applying the exact kinematic boundary condition of no normal flow at solid walls rather than imposing conditions such as no normal geostrophic flow, which is an error of order Rossby number.

The model we describe is based around a predictor-corrector approach. It is first developed and tested for cases with strictly positive layer thickness. The model is then modified to cope with zero layer thickness ('outcropping'). A flux limiting scheme is used to prevent regions of negative mass from being formed.

Although we emphasize the numerical formulation, we compare our model results with the analytic outcropping solutions of Parsons(1969) and the numerical solutions of Bogue, Huang and Bryan(1986) and Huang(1986). Good agreement is observed. Finally the model is used to look at a situation where both inertia and outcropping are important.

# 1 Introduction

A major deficiency of many previous idealised ocean models has been their neglect of non-linearities in either (or both) the momentum equations or the continuity equation. For example the quasi-geostrophic equations include inertial non-linearity, but ignore much of the non-linearity associated with change in isopycnal layer thickness. Much recent interest has been shown in intermediate models (*e.g.* Gent and McWilliams 1983, Allen *et al.* 1990). These remedy this difficulty by choosing a balance intermediate between quasi-geostrophic equations and the primitive equations while using a better approximation to the continuity equation.

In this paper the shallow water form of the semi-geostrophic equations (sometimes called the geostrophic momentum approximation equations (Eliassen 1948)) is used as a basis for a numerical ocean model. These equations have the properties of retaining most of the non-linearity in the momentum equations while including all of the non-linearity in the continuity equation. They also do not support gravity waves. The shallow water form is a prototype for a many layer isopycnal model (*e.g.* Bleck and Boudra 1986). The model is intended for, though not restricted to, highly idealised studies of a rectangular ocean on a beta plane. The technique can be applied to many other balanced equation sets. The model we describe is capable of modelling the outcropping of density surfaces as occurs when the thickness of the shallow water layer becomes vanishingly small.

Allen *et al.*(1990) and Barth *et al.*(1990) have recently evaluated many intermediate models in both analytic and numerical situations. They plotted the Rossby number against error (the difference between the balanced solution and the solution to the primitive equations). In the specific cases they studied the semi-geostrophic equations perform relatively poorly. But they did note that the accuracy of the semi-geostrophic approximation was mostly unchanged as layer thickness variations increased, whereas many of the other intermediate

models performed increasingly badly. The semi-geostrophic equations differ from most other balanced models studied by Allen *et al.* and Barth *et al.* in relying only on the smallness of the Lagrangian Rossby number. In some cases this can differ greatly from the Eulerian Rossby number which is required to be small for other balanced models. This suggests that the Eulerian Rossby number used in the studies of Allen *et al.* and Barth *et al.* is not necessarily the most important parameter in studying the accuracy of balanced models, other choices are clearly possible.

We consider the semi-geostrophic equations to be an interesting set to integrate not least because of the unambiguous way in which the boundary conditions are applied. Many other sets of intermediate models require the kinematic boundary condition to be partitioned between either the geostrophic and ageostrophic flow (*e.g.* the quasi-geostrophic equations) or between the rotational and divergent flow (*e.g.* McWilliams *et al.* 1990). The frequently used boundary conditions of imposing both streamfunction and velocity potential to be constant is an order Rossby number error. Much of our ultimate interest is in solutions where the layer thickness varies greatly over the basin. The boundary conditions are vital in these situations. The semi-geostrophic approximation formulation used here imposes the exact kinematic boundary condition of no normal flow at solid walls.

The semi-geostrophic equations have useful analogues of the conservation laws for energy, vorticity and potential enstrophy on an  $f$ -plane. Moreover existence and uniqueness proofs (Cullen and Purser 1989) and the many properties of the differential equations on an  $f$  plane make the set well posed and mathematically tractable. In situations where the Coriolis parameter varies spatially there are several semi-geostrophic options. Salmon (1985), Shutts (1989) and Magnusdottir and Schubert (1990) have all introduced forms of the semi-geostrophic equations which all limit to the original set if  $f$  is constant. Here we choose a simpler option. We retain the original semi-geostrophic

momentum equations and allow the Coriolis parameter to vary spatially.

In this paper we present a finite difference numerical model of the ocean based upon the shallow water form of the semi-geostrophic momentum equations. The model can cope with the shallow water layer disappearing and is a one layer version of a multi-layer isopycnal ocean model. The main purpose of this paper is to demonstrate the numerical techniques and to verify the accuracy of the model in some sample steady situations. We will also extend some of the outcropping results of Bogue *et al.* (1986) into regimes with greater inertial non-linearity. Future papers will apply this model to study new physical situations.

### 1.1 The Semi-Geostrophic Approximation

The semi-geostrophic approximation was first introduced by Eliassen (1948). Hoskins (1975) derived these equations from a consistent approximation and applied them in suitably transformed coordinates. These equations are obtained by replacing the full momentum in the horizontal momentum equations by the geostrophic momentum. In shallow water form, the equations are

$$\frac{Du_g}{Dt} - fv + fv_g = 0, \quad (1)$$

$$\frac{Dv_g}{Dt} + fu - fu_g = 0, \quad (2)$$

where the pressure gradients have been replaced with geostrophic velocities given by,

$$fv_g = g' \frac{\partial h}{\partial x}, \quad (3)$$

$$-fu_g = g' \frac{\partial h}{\partial y}. \quad (4)$$

where  $g'$  is the reduced gravity and  $f$ , the Coriolis parameter, is allowed to vary. The continuity equation is the shallow water form

$$\frac{Dh}{Dt} + h \nabla \cdot \underline{v} = 0. \quad (5)$$

for a layer of constant density and thickness  $h$ . Where

$$\frac{D}{Dt} = \frac{\partial}{\partial t} + u \frac{\partial}{\partial x} + v \frac{\partial}{\partial y}. \quad (6)$$

The semi-geostrophic approximation is obtained in the limit where the Lagrangian Rossby number is small, that is

$$\frac{\left| \frac{D}{Dt} \left( \frac{1}{f} \frac{Du}{Dt} \right) \right|}{|fu|} \ll 1, \quad (7)$$

and

$$\frac{\left| \frac{D}{Dt} \left( \frac{1}{f} \frac{Dv}{Dt} \right) \right|}{|fv|} \ll 1. \quad (8)$$

see Hoskins (1975)

These conditions are typical for balanced models, which normally require small Eulerian Rossby number (*e.g.* McWilliams and Gent 1980). The accuracy of these equations is independent of the stratification. The more common quasi-geostrophic equations linearise about a constant layer thickness, this is not necessary here. These equations are hence capable of representing isopycnal surfacing and separation processes such as occur in the Gulf Stream.

The equations have the following properties.

- They conserve energy.
- Boundary conditions can be applied at solid boundaries in a natural manner.
- They have the full continuity equation for a single shallow water layer of constant density. This allows us to study situations allowing outcropping.
- They do not support gravity waves.

Although we are interested in integrating these equations forward on a beta plane, in the special case of an  $f$ -plane the equations have the following additional properties.

- They conserve analogues of potential vorticity and potential enstrophy.
- They have existence and uniqueness proofs (Cullen and Purser 1989).  
No diffusion is required to close the equations.
- They can be derived from the Hamiltonian (Salmon 1985).

A consequence of the variable Coriolis parameter is that there is no vorticity conservation law, hence we cannot use the semi-geostrophic coordinate transform of Hoskins(1975).

We instead choose a predictor-corrector approach similar to that used by (Cullen 1989a) to integrate the momentum, continuity and geostrophic balance equations forward in time. Other authors (Salmon 1985, Shutts 1989, Magnusdottir and Schubert 1990) have introduced semi-geostrophic equations which in the limit of constant  $f$  are the equations (1 - 6) but which maintain a conservation law for vorticity in the case of a variable Coriolis parameter. These sets can be integrated forward in time using the coordinate transform of Hoskins(1975). We were unable to develop a stable numerical scheme using this approach because solid ocean walls are not stationary in the transformed coordinate system.

The approach used here can be applied to many other balanced sets with minimal difficulty. In particular the approach used here to solve our equations could very simply be modified to solve the Shutts equations. Our choice of eqs. (1 - 6) is motivated by their closer resemblance to the shallow water equations, than any of these other sets. It is also easy to see how to write these equations in many layer form or with a different vertical coordinate (*e.g.* height or  $\sigma$ ), and that extensions to a full ocean model with many vertical layers (or levels) are relatively simple.

## 2 Integration of the Semi-Geostrophic Equations

The equations are to be solved in a rectangular basin with a prescribed wind forcing distributed over the thickness of the layer. The momentum sink is of linear drag form acting upon the geostrophic velocity only. This closes the energy equation and represents dissipation by vertical shearing of horizontal velocities. This formulation is used to guarantee that the drag always acts to reduce the energy (Cullen 1989b).

In this paper we look mostly at a sub-tropical gyre representing the north Atlantic. Various values of stratification, wind and the Coriolis parameter are studied.

Before we describe the solution technique, it is useful to write the equations in non-dimensional form. The semi-geostrophic equations (1-6) are first written in mass transport form (*i.e.* where eqs. 1 and 2 are multiplied by  $h$  and the velocity  $\underline{v}$  substituted by the mass transport  $\underline{V} = \underline{v}h$ ). Our numerical model is formulated using mass transport as a prognostic variable. Source terms representing the wind and linear drag friction are then introduced into the  $x$  and  $y$  momentum equations respectively as  $(\tau_x - \epsilon u_g)$  and  $(\tau_y - \epsilon v_g)$ . With this form of dissipation only one boundary condition (no flow through walls) is required at the basin edge. No condition is required on the tangential flow.

Scales are specified for  $\underline{V}, \underline{v}_g, h, t, x$  and  $f$  as  $(v_0 h_0), v_0, h_0, f_0^{-1}, L$  and  $f_0$  respectively. The semi-geostrophic equations in non-dimensional variables become

$$h \frac{\partial u_g}{\partial t} + R_o U \frac{\partial u_g}{\partial x} + R_o V \frac{\partial u_g}{\partial y} - f' V + f' v_g h = \tau_M \tau'_x - \epsilon' u_g \quad (9)$$

$$h \frac{\partial v_g}{\partial t} + R_o U \frac{\partial v_g}{\partial x} + R_o V \frac{\partial v_g}{\partial y} + f' U - f' u_g h = \tau_M \tau'_y - \epsilon' v_g \quad (10)$$

$$\frac{\partial h}{\partial t} + R_o \left( \frac{\partial U}{\partial x} + \frac{\partial V}{\partial y} \right) = 0 \quad (11)$$

$$R_o f' v_g = B_u \frac{\partial h}{\partial x} \quad (12)$$

$$-R_o f' u_g = B_u \frac{\partial h}{\partial y} \quad (13)$$

where

$$R_o = \frac{v_0}{f_0 L}, \quad (14)$$

is the Rossby number and

$$B_u = \frac{g' h_0}{f_0^2 L^2}, \quad (15)$$

is the Burger number, a measure of the stratification. The number

$$\epsilon' = \frac{\epsilon}{f_0 h_0} \quad (16)$$

is the non-dimensional coefficient of linear drag, wind forcing is non-dimensionalised using

$$\tau_M \tau'_x = \frac{1}{f_0 v_0 h_0} \tau_x(x, y) \quad (17)$$

$$\tau_M \tau'_y = \frac{1}{f_0 v_0 h_0} \tau_y(x, y) \quad (18)$$

where  $\tau_x(x, y)$  and  $\tau_y(x, y)$  are the dimensional wind stresses,  $\tau_M$  is a constant and  $\tau'_x$  and  $\tau'_y$  are order one functions of space.

Choosing  $f_0 = \beta L$  to help the physical interpretation of non-dimensional parameters gives  $f' = \gamma + y'$  where  $\gamma = f_{REF}/\beta L$ , a measure of the variation of  $f$  over the basin,  $y'$  is the non-dimensional latitude and  $f_{REF}$  is  $f$  where  $y' = 0$ . This choice of  $f_0$  also leads to  $R_o = (L_I/L)^2$ ,  $B_u = (L_\rho/\gamma L)^2$  and  $\epsilon' = L_\epsilon/L$  where  $L_I, L_\rho, L_\epsilon$  and  $L$  are the inertial length scale ( $= (v_0/\beta)^{1/2}$ ), the Rossby radius ( $= \sqrt{g'h_0}/f_{REF}$ ), the scale of a frictional boundary current ( $= \epsilon/\beta h_0$ ) and the length of the basin respectively.

We choose to scale the velocity using the maximum Sverdrup transport, for the wind stress ( $\tau_x = -\tau_0 \cos(\pi y/L), \tau_y = 0$ ) then

$$\beta v_0 h_0 \sim \frac{\pi \tau_0}{L} \quad (19)$$

and

$$\tau_M \tau'_x = -\frac{1}{\pi} \cos(\pi y') \quad (20)$$

## 2.1 The Finite Difference Equations

Here we present the finite difference equations to be solved, the grid they are to be solved upon and the boundary conditions they have.

The variables are arranged on the grid (fig. 1) which has  $N_X$  h points in the  $x$  direction and  $N_Y$  h points in the  $y$  direction. The grid lengths in the  $x$  and  $y$  direction are  $\Delta x$  and  $\Delta y$  respectively such that  $\Delta x = 1/(N_X)$  and  $\Delta y = 1/(N_Y)$ . The mass transport is calculated on an Arakawa 'C' grid (Arakawa, 1972), and the geostrophic velocities on the Arakawa 'D' grid. This choice has the advantage of representing redistribution of mass accurately while being a natural grid for the evaluation of geostrophic pressure gradients, but it has the disadvantage of averaging the pressure gradient terms of the momentum equations.

The discretised variables will be denoted by  $A_{i,j}^n$  which is the value of the variable  $A$  at the  $i$ th grid point in the  $x$  direction and the  $j$ th grid point in the  $y$  direction at the time  $n\Delta t$  where  $\Delta t$  is the time step. We define the usual delta and bar finite difference operators

$$\delta_x A = \frac{(A_{i+1/2,j} - A_{i-1/2,j})}{\Delta x} \quad (21)$$

and

$$\bar{A}^x = \frac{A_{i+1/2,j} + A_{i-1/2,j}}{2} \quad (22)$$

with the obvious equivalents in the  $y$  direction and  $\delta_{2x} A$  being the equivalent of  $\delta_x A$  over 2 grid lengths. Variables with no time labels are assumed to be at time level  $n$ . The time scheme we use is an Euler step for the first time step followed by a leapfrog scheme for all subsequent steps. An Asselin-Robert time filter (Asselin 1972, Robert 1966) is used at the end of each step on  $u_g$ ,  $v_g$  and  $h$  to remove the computational modes of the leapfrog scheme. The non-linear (advection) terms are written in a quadratic conservative form so that momentum ( $hu_g$ ) is changed by a flux type equation and the friction term is calculated from values at the new time step. This is to enhance numerical

stability especially as  $h$  approaches zero. The finite difference equations we solve are

$$\bar{h}^y \left( \frac{u_g^{n+1} - u_g^{n-1}}{2\Delta t} \right) + R_o \overline{U^y} \delta_x u_g^x + V(R_o \delta_{2y} u_g - f') + \overline{f' v_g^{xy}} \bar{h}^y = -\epsilon' u_g^{n+1} + \tau_M \tau_x' \quad (23)$$

$$\bar{h}^x \left( \frac{v_g^{n+1} - v_g^{n-1}}{2\Delta t} \right) + U(R_o \delta_{2x} v_g + f') + R_o \overline{V^x} \delta_y v_g^y - \overline{f u_g^{xy}} \bar{h}^x = -\epsilon' v_g^{n+1} + \tau_M \tau_y' \quad (24)$$

$$\left( \frac{h^{n+1} - h^{n-1}}{2\Delta t} \right) + R_o (\delta_x U + \delta_y V) = 0 \quad (25)$$

$$-R_o f' v_g + B_u \delta_x h = 0 \quad (26)$$

$$R_o f' u_g + B_u \delta_y h = 0 \quad (27)$$

So that eqs. (23) and (27) are evaluated at  $u_g$  points on the grid, (24) and (26) are evaluated at  $v_g$  points and (25) is evaluated at  $h$  points.

The boundary conditions are that there is no mass flux through the walls. This is a significant advantage over many other balanced models which either impose conditions on the geostrophic velocity at the boundary (e.g. the quasi-geostrophic equations impose  $v_g \cdot \hat{n} = 0$ ) or false conditions upon the divergent or non-divergent parts of the flow (e.g. McWilliams *et al.* 1990 who impose both streamfunction and velocity potential as zero). These alternative boundary conditions are often in error at order Rossby number. This becomes especially important as the layer thickness variation increase.

## 2.2 Solving the Finite Difference Equations

The technique used to solve these equations is somewhat similar to that used to solve the Navier-Stokes equations, where the pressure is corrected to ensure that the velocity divergence is zero at the new time step (Williams 1969). Here, following Cullen (1989a), we correct the full mass transports to enforce geostrophic balance between the pressure and geostrophic velocities at the new time level. The eqs. (23-27) form a closed set of 3 prognostic and 2 diagnostic finite difference equations in five variables. The 3 prognostic equations give

new values of  $u_g, v_g$  and  $h$ . But there is no prognostic equation for new values of the full mass transports  $U$  and  $V$ . Therefore an implicit equation has to be solved, at some point in the procedure, for the new values of these variables. The values of  $U$  and  $V$  required are those which make the prognostically calculated variables  $u_g, v_g$  and  $h$  satisfy the 2 diagnostic definitions of geostrophic balance, eqs.(26) and (27), at the end of the time step.

This numerical scheme works in two stages, first ensuring that  $v_g$  and  $\delta_x h$  satisfy eq.(26) by adjusting  $U$ , and then by ensuring that  $u_g$  and  $\delta_y h$  satisfy eqn. (27) by adjusting  $V$  and repeating until satisfactory convergence is obtained.

The scheme is similar to solving equations (23 -27) by alternating direction implicit (ADI) methods or by line relaxation in the Gauss-Seidel approach. To demonstrate the technique we describe one iteration.

Evaluation of  $U$  consists of making a guess for  $v_g$  and  $h$  using values from the previous time steps, and finding the small changes in  $U$  which would enforce geostrophy in these new fields if  $v_g$  and  $h$  were recalculated using eqs.(24 and 25).

At the end of the previous time step ( $n$ ) all the fields ( $u_g^n, v_g^n, h^n, U$  and  $V$ ) are known and the diagnostic relations (26 and 27) have been satisfied by these geostrophic velocities and layer thickness fields. These variables and the ones from the previous time step ( $n - 1$ ) are then used in (24 and 25) to get trial values of  $v_g$  and  $h$  at the new time level ( $n + 1$ ). These values will be denoted here by  $v_g^\#$  and  $h^\#$ . This trial step can be written

$$\bar{h}^x \left( \frac{v_g^\# - v_g^{n-1}}{2\Delta t} \right) + U(R_o \delta_{2x} v_g + f') + R_o \overline{V^x} \delta_y v_g^y - \overline{f' u_g^{xy}} \bar{h}^x = -\epsilon' v_g^\# + \tau_M \tau_y' \quad (28)$$

$$\left( \frac{h^\# - h^{n-1}}{2\Delta t} \right) + R_o (\delta_x U + \delta_y V) = 0 \quad (29)$$

At boundaries we do not integrate for the geostrophic flow parallel to the wall so that where  $U = 0$ ,  $v_g$  is not calculated and at a wall where  $V = 0$ ,  $u_g$  is not calculated. Where boundary values of  $u_g$  and  $v_g$  are needed to evaluate

the non-linear terms in the momentum eqs. (23 and 24) they are linearly extrapolated from the interior values. This is equivalent to side differencing.

Since the mass transports ( $U, V$ ) are from the previous time step (or iteration) it can be seen that in general the values given by (28) and (29) do not satisfy the geostrophic balance relation (27). Namely

$$-R_o f' v_g^\# + B_u \delta_x h^\# = -R_1 \neq 0 \quad (30)$$

Where  $R_1$  is known as the residual and is evaluated at  $v_g$  points on the grid (fig. 1). The task now is to find the small changes to  $U$  so that if this step is redone  $R_1$  is zero.

For a given change in the mass transport ( $\delta U$ ), the change in the result of the prognostic steps (28-29) is given by linearisation. This results in

$$\left( \frac{\bar{h}^x}{2\Delta t} + \epsilon' \right) \delta v_g + \delta U (R_o \delta_{2x} v_g + f') = 0 \quad (31)$$

$$\left( \frac{\delta h}{2\Delta t} \right) + R_o \delta_x \delta U = 0 \quad (32)$$

where  $\delta v_g$  and  $\delta h$  are the differences between the  $\#$  values and the values obtained if  $U$  was changed by  $\delta U$ . We require that this  $\delta U$  should lead to the removal of the residuals  $R_1$  in Eq. (30). Hence

$$-R_o f' (v_g^\# + \delta v_g) + B_u \delta_x (h^\# + \delta h) = 0 \quad (33)$$

Subtracting (30) from this leads to

$$-R_o f' \delta v_g + B_u \delta_x (\delta h) = R_1 \quad (34)$$

The 3 linear equations (31,32 and 34) for the 3 unknowns ( $\delta U, \delta v_g$  and  $\delta h$ ) can be solved given the correct boundary conditions ( $\delta U = 0$  at east and west walls). These are combined to give

$$\frac{\delta h}{2\Delta t} + \delta_x \left[ \frac{(R_1 - B_u \delta_x (\delta h))}{f' (f' + R_o \delta_{2x} v_g)} \left( \frac{\bar{h}^x}{2\Delta t} + \epsilon' \right) \right] = 0 \quad (35)$$

which is  $N_Y$  tridiagonal matrix inversions each for the  $N_X$   $\delta h$  values of a row.

Elimination of  $\delta v_g$  between Eq.(31) and (34) gives

$$R_o \delta U = \frac{(R_1 - B_u \delta_x(\delta h))}{f'(f' + R_o \delta_{2x} v_g)} \left( \frac{\bar{h}^x}{2\Delta t} + \epsilon' \right) \quad (36)$$

which relates  $\delta U$  with  $\delta h$  and other quantities known after the predictor stage.

The solution  $\delta h$  from (35) is substituted back into eq.(36) to obtain  $\delta U$  which is then added onto  $U$ .

The evaluation of  $V$  follows a similar procedure. We solve

$$\frac{\delta h}{2\Delta t} + \delta_y \left[ \frac{(R_2 - B_u \delta_y(\delta h))}{f'(f' - R_o \delta_{2y} u_g)} \left( \frac{\bar{h}^y}{2\Delta t} + \epsilon' \right) \right] = 0 \quad (37)$$

where  $R_2 = -R_o f u_g^\# - B_u \delta_y h^\#$ . This is  $N_X$  tridiagonal matrix inversions each for the  $N_Y$   $\delta h$  values of a column. The equation relating  $\delta h$  and  $\delta V$  is

$$R_o \delta V = \frac{(R_2 - B_u \delta_y(\delta h))}{f'(f' - R_o \delta_{2y} u_g)} \left( \frac{\bar{h}^y}{2\Delta t} + \epsilon' \right) \quad (38)$$

The correction  $\delta h$  from eq.(37) is inserted into eq.(38) to obtain  $\delta V$  and hence the new  $V$ .

The loop of doing trial steps for  $v_g$  and  $h$  and correcting  $U$  to satisfy geostrophy followed by doing trial steps for  $u_g$  and  $h$  and correcting  $V$  to satisfy geostrophy, is repeated until the residuals  $R_1$  and  $R_2$  are sufficiently small (see fig. 2). If the residuals were exactly zero then we would have precisely solved the finite difference equations(23-27). We then proceed to the next step.

The iteration is necessary because updated values of mass transport have not been included in the perpendicular direction. After evaluating a new  $V$  using eq.(37) and (38) reevaluation of eqs. (28) and (29) will result in the residual  $R_1$  in eq.(30) not being zero. After the final iteration, all predictor steps are redone to include the latest and best values of mass transport. Each tridiagonal matrix inversions requires only order  $N$  calculations for problem of length  $N$ .

This method of solution can be very cheap although if a high level of convergence is not obtained, the spin-up process may be slowed down (Clove 1992). An alternative method that can solve these equations very accurately is to solve for  $\delta U$  and  $\delta V$  simultaneously using

$$\frac{\delta h}{2\Delta t} + \delta_x \left[ \frac{(R_1 - B_u \delta_x(\delta h))}{f'(f' + R_o \delta_{2x} v_g)} \left( \frac{\bar{h}^x}{2\Delta t} + \epsilon' \right) \right] + \delta_y \left[ \frac{(R_2 - B_u \delta_y(\delta h))}{f'(f' - R_o \delta_{2y} u_g)} \left( \frac{\bar{h}^y}{2\Delta t} + \epsilon' \right) \right] = 0 \quad (39)$$

This requires a variable coefficient elliptic inversion for the  $\delta h$ 's. This is much more expensive than the tridiagonal inversion approach we use here. One elliptic inversion takes a minimum of  $N \log N$  calculations for an  $N$  gridpoint domain, whereas the tridiagonal inversions we require here are accomplished in order  $N$  calculations. In this paper only steady solutions are examined and so an error in the spin-up scale is unimportant.

The semi-geostrophic equations can be integrated forward in time validly, only when the vorticity is positive. The equivalent numerical requirement is that

$$(f' - R_o \delta_{2y} u_g)^n > 0 \quad (40)$$

and

$$(f' + R_o \delta_{2x} v_g)^n > 0 \quad (41)$$

at all  $h$  points. The full algorithm is shown in fig. (2)

### 3 Model Runs

Here we look at solutions from the model. In the limit of very large mean depth compared to layer thickness variations, the shallow water continuity equation tends to the non-divergent equation  $\nabla \cdot \mathbf{u} = 0$ . For idealised wind forcing, solutions similar to those of Veronis(1966) are expected. Figures (4-5) show some solutions where the layer thickness varies very little from the mean and the wind forcing has the dimensional form  $(\tau_x = -0.5\tau_0 \sin(\pi x/L) \cos(\pi y/L), \tau_y =$

$0.5\tau_0 \cos(\pi x/L) \sin(\pi y/L)$ ). We show both the layer thickness and the streamfunction. The streamfunction is derived by noting that the mass transport is non-divergent in the steady state (from eq. 11). This is true even if the layer thickness varies greatly.

The geostrophic flow cannot cross layer thickness contours and the mass transport cannot cross streamlines. Figures (4 and 5) show the layer thickness and streamfunction in the case of very small Rossby number (table 1, shows the non-dimensional parameters). In this regime the momentum equations (9 and 10) become linear, and the classic Stommel (1948) gyre is reproduced. A marked difference between streamlines and layer thickness contours is obtained. The streamlines do not intersect the walls whereas the layer thickness contours hit the wall. This is because of the different boundary conditions on these fields. The streamfunction is zero at the walls and the layer thickness satisfies a balance between the geostrophic flow the Ekman terms and the friction. On the northern wall, for example, this is

$$\frac{1}{2} \frac{B_u}{R_o} \frac{\partial h^2}{\partial x} = \frac{1}{\pi} \tau_x' + \frac{\epsilon'}{f'} \frac{B_u}{R_o} \frac{\partial h}{\partial y} \quad (42)$$

since  $v = 0$ . The more common quasi-geostrophic equations are typically integrated, in a closed basin, with the layer thickness fixed on the boundary (e.g. Marshall *et al.* 1988)

Figures (6–8) show successively higher Rossby numbers and the purely western boundary current of figs. (4–5) slowly transforms into a more inertial current. As the Rossby number gets higher (relative to  $f'$ ) the iteration scheme implicit in the correction loops evaluating the new velocities becomes less rapidly convergent. If locally the relative vorticity becomes larger than  $f'$ , the iteration may diverge and the model will fail. There is also a weak non-linear numerical instability associated with the terms like  $V \partial u_g / \partial y$  which can also cause convergence difficulties. A solution to this problem might be to use a positive definite advection scheme such as flux corrected transport (FCT) Zalesak (1979).

Figure (9) shows a run where the stratification is much weaker ( $B_u$  is small). The layer thickness variations are much larger in this case, (the Rossby number and the frictional coefficient are the same as in fig. 6 ) so that the ratio of thinnest to thickest values is about three. The boundary current has a significantly more inertial form than fig. (6 ). Since the layer thickness in the western boundary current is greater than one, the frictional terms are less effective and the boundary current travels noticeably further around the boundary. As the stratification gets weaker then the layer thickness variations increase. Another important effect is the slowing down of the Rossby waves as layers get thinner or the Burger number gets smaller. It can be shown (Clove 1992) that the Rossby wave speed for these equations (for zero meridional wavenumber) is given by

$$c_p = \frac{\omega}{k} = \left( \frac{B_u h (R_o u f'^2 - 1)}{B_u h k^2 + f'^2} \right) \quad (43)$$

When the Burger number or the layer thickness  $h$  is small their speed is  $-B_u h / f'^2$  relative to the mean flow. In quasi-geostrophic models (where  $B_u$  should be about 1 for validity) the speed is  $-1/(k^2 + (B_u)^{-1})$  and in a barotropic non-divergent model it is  $-1/k^2$ . Typically, Rossby waves in quasi-geostrophic and barotropic non-divergent models are more rapid than those in an isopycnal model with weak stratification or thin layers. The spin-up to steady state, which depends upon these Rossby waves, may take several years even without eddies. It is this slow Rossby wave speed which makes isopycnal models with weak stratification (or thin layers) take much longer to spin-up to a Sverdrup type balance than their quasi-geostrophic counterparts.

In the extreme case the thickness reaches zero. The formulation of the model presented in section 2 takes no account of this and will integrate the equations regardless. In the following section we describe the modifications required to make this model cope with this 'outcropping' without allowing negative values of layer thickness.

## 4 Outcropping Modifications

Here we describe modifications to our model enabling it to cope with the drying up of the single shallow water layer. This 'drying up' represents the outcropping of deeper density layers. As far as we are aware, this is the only balanced model which allows the drying up of isopycnal layers.

Other isopycnal models (*e.g.* the Bleck and Boudra 1986 model) cope with surfacing isopycnals by using the flux corrected transport scheme, applied to the continuity equation, to redistribute mass. Flux corrected transport (FCT) schemes (Boris and Book 1973, Zalesak 1979) remove the possibility of negative layer thickness by locally changing the formulation of the mass flux in the continuity equation, in those places on the grid where negative layer thicknesses (and other spurious maxima or minima) are likely to occur. The FCT scheme uses a combination of a first order accurate upwind formulation, and a higher order formulation. The combination is chosen so that no new maxima or minima (of the final fields) are formed that did not already exist at the previous step or would not be produced by the upwind scheme alone. Since the upwind formulation has the property of being unable to create negative values of  $h$  (if the CFL criterion is satisfied), and the initial  $h$  field is positive then the FCT scheme maintains  $h$  as being positive.

Although flux corrected transport schemes are numerically robust and are frequently used in numerical modelling, they are not suitable for use with our model formulation. Where flux limiting occurs the FCT type schemes change the finite differencing. The difference scheme for each point is not chosen until the direction and strength of the final velocities are known. The predictor-corrector scheme we use is based around linearisation of the finite difference scheme and depends upon knowing the finite differencing *before* we can formulate the inversion to evaluate the final velocities. Hence the pure FCT scheme is not applicable, although some of its concepts can be used to develop a scheme which allows outcropping.

The scheme we describe, evaluates the mass transports required to fully remove the residuals and adjust as few of these as possible while guaranteeing that we do not create any negative values of  $h^{n+1}$ . The final distribution of mass is as close as possible to the zero residual solution. Our scheme differs from the FCT schemes in requiring only that the new fields are non-negative.

The initial predictor stage, is treated somewhat differently from subsequently stages, we limit the full mass flux, to ensure no negative values of  $h$  are created. In subsequent stages we need limit only the change in fluxes to ensure positivity of  $h$ . The residual calculation and inversion are left unaltered.

#### 4.1 The Flux limiting scheme

Our scheme evaluates the net flux from a box which would make the box have zero mass (for the initial predictor step this is  $h^{n-1}\Delta x/2\Delta t$ ). If the sum of the fluxes out of this box is greater than this, then the outward fluxes are limited and this new value is used in the momentum equation. These modified fluxes must be used in the momentum equation to retain the consistency of the linearisation technique.

Generally for the initial predictor step we define, for each  $h$  gridpoint, the ratio (between 0 and 1) of *outward* fluxes that would *alone* just cause outcropping. For each  $h$  point this ratio  $\alpha_{i,j}$  is given by

$$\frac{-h_{i,j}^{n-1}}{2\Delta t} + R_o\mu_{i,j} \left( \frac{\max(0, U_{i+1,j}) - \min(0, U_{i,j})}{\Delta x} + \frac{\max(0, V_{i,j+1}) - \min(0, V_{i,j})}{\Delta y} \right) = 0 \quad (44)$$

$$(45)$$

and

$$\alpha_{i,j} = \min(0, \mu_{i,j}) \quad (46)$$

We limit only the outward fluxes, so these are the only fluxes included in this calculation. Inward fluxes are not adjusted because they might themselves be

altered by the competing requirement that the box they leave must remain non-negative. The limited fluxes we use are,

$$U_{i,j}^L = \alpha_{i-1,j} \max(0, U_{i,j}) + \alpha_{i,j} \min(0, U_{i,j}) \quad (47)$$

$$V_{i,j}^L = \alpha_{i,j-1} \max(0, V_{i,j}) + \alpha_{i,j} \min(0, V_{i,j}) \quad (48)$$

where the relevant  $\alpha$  is taken from the box the flux is leaving. These limited fluxes are then used to evaluate  $h^\#$  and  $v_g^\#$  the predicted values of  $h^{n+1}$  and  $v_g^{n+1}$  using

$$\frac{h^\# - h^{n-1}}{2\Delta t} + R_o(\delta_x U^L + \delta_y V^L) = 0 \quad (49)$$

$$\bar{h}^x \left( \frac{v_g^\# - v_g^{n-1}}{2\Delta t} \right) + U^L (R_o \delta_{2x} v_g + f') + R_o \overline{V^L}^x \delta_y v_g - f' u_g^x \bar{h}^x = -\epsilon' v_g^\# + \tau'_M \tau'_y \quad (50)$$

as in the non-outcropping scheme. The residual (30) is then evaluated and  $\delta U$  calculated using eqs.(35-36)

## 4.2 Flux Limiting at subsequent Stages

At subsequent stages, after the inversions provide a change in mass fluxes  $\delta U$  or  $\delta V$ , only this flux change need be limited. Since we know that the previous values  $U^L$  or  $V^L$  do not produce negative  $h^\#$ , any values of  $h^\# < 0$  must result from the  $\delta U$  or  $\delta V$  increment.

For a change in mass flux  $\delta U$   $h^\#$  changes according to,

$$\frac{\Delta h}{2\Delta t} + R_o \delta_x \delta U = 0 \quad (51)$$

where  $\Delta h = (\text{Value after correction} - h^\#)$ . The flux limiting appropriate to this must ensure that  $\Delta h$  is greater than  $-h^\#$  where  $h^\#$  is the best previously known  $h$ .

For each trial value of  $h_{i,j}^\#$  we evaluate the ratio of outward fluxes that would exactly cause outcropping, this is the  $\alpha_{i,j}$  which satisfies

$$\frac{-h_{i,j}^\#}{2\Delta t} + R_o\mu_{i,j} \left( \frac{\max(0, \delta U_{i+1,j}) - \min(0, \delta U_{i,j})}{\Delta x} \right) = 0 \quad (52)$$

and

$$\alpha_{i,j} = \min(0, \mu_{i,j}) \quad (53)$$

hence the limited (change in) fluxes are evaluated using

$$\delta U_{i,j}^L = \alpha_{i-1,j} \max(0, \delta U_{i,j}) + \alpha_{i,j} \min(0, \delta U_{i,j}) \quad (54)$$

and new full fluxes calculated using

$$U_{i,j}^L = U_{i,j} + \delta U_{i,j}^L \quad (55)$$

where  $U_{i,j}$  was used to produce  $h^\#$  and is the best known flux from either the previous time step or iteration. We use these new limited fluxes to evaluate new values of  $h^\#$  with

$$\frac{h_{i,j}^\# - h_{i,j}^{n-1}}{2\Delta t} + R_o(\delta_x U^L + \delta_y V) = 0 \quad (56)$$

A similar scheme applies for increments  $\delta V$ .

The same structure of iteration is used as in the non-outcropping model except for this flux-correction scheme being used to redistribute the mass. The algorithm is presented in figure (3).

Using this scheme we will not remove all of the residuals at points on the grid where flux limiting occurs. In classical problems where the equations cannot be satisfied exactly at discontinuities, adjacent residuals are ignored. In this case it is unclear before the inversion whether the fluid will outcrop and whether the equations can be exactly satisfied at each grid box. Hence we cannot just ignore the residual at outcropping boxes which will outcrop at the inversion stage. We choose to solve the exact equations in the inversions and modify the fluxes and residuals afterwards. Since the flux limiting adjusts

fluxes, some non-zero residuals are inevitable. In practice if we leave these residuals non-zero they grow and ultimately cause model failure. We circumvent this difficulty by making use of our balance condition ( $v_g = g'\delta_x h/f$ ) to evaluate  $v_g^{n+1}$  near flux limited points after the rest of the step has been completed.

Near flux limited points the geostrophic flow is not obtained by the prognostic integration, of the momentum equations. Although this scheme leads to the best value of mass transport consistent with non-negative layer thickness, and hence the best possible distribution of mass, the exact balances at the outcrop edge are not necessarily consistent with the momentum equations. The exact quadratic momentum flux conservation is lost at the outcrop edge. A similar problem is discussed by Bleck and Boudra (1986).

Although there is guaranteed to be a unique solution to the continuous semi-geostrophic equations (on an f-plane) with all non-negative mass (Cullen and Purser 1989) the unique solution to the finite difference equations can, at times, involve negative layer thickness. As the Rossby number increases, the source/sink of momentum implied by the imposition of geostrophy at outcropped points may have a larger effect on the interior flow. A better condition upon the geostrophic velocity at the outcrop edge is clearly required.

## 5 Solutions with Outcropping

In this section we show solutions from our outcropping model. We first reproduce a known result. Initially we configure the model to compare solutions both with the numerical results of Bogue, Huang and Bryan(1986)(hereafter BHB) and the analytic solutions of Parsons(1969). The wind forcing is purely zonal ( $\tau_x = -\tau_0 \cos(\pi y/L)$ ,  $\tau_y = 0$ ), and the non-dimensional parameters are  $(3.1 \times 10^{-4}, 1.64 \times 10^{-4}, 2 \times 10^{-2}, 1.4)$  respectively for  $R_o$ ,  $B_u$ ,  $\epsilon'$  and  $\gamma$ . These correspond to inertial and frictional length scales of 1/57 and 1/50 of the basin respectively. There are 80 gridpoints in each direction in each model.

The BHB model integrates the shallow water equations forward in time, omitting the non-linear advection terms and the time-derivative term in each momentum equation. They use a linear drag frictional dissipation. If there is a unique steady state then in the limit of small Rossby number, solutions to our model (which includes momentum advection) should coincide with those of BHB (although in their model friction acts on the full velocity and in ours on the geostrophic velocity).

Fig.(10) shows the (non-dimensional) layer thickness from our model. The parameters (see table 1) are set up to reproduce figure (1b) of BHB (which we reproduce as our fig. 11). This solution has a low Rossby number but has a large outcropped region in the north-west corner of the basin, south of which is the separated boundary current representing the Gulf stream.

In our solution the minimum layer thickness is exactly zero suggesting that our flux limiting scheme is accurately maintaining the non-negative nature of the fields. Over much of the outcropped region the layer thickness is of order  $10^{-3}$  relative to the mean (which is 1 in all figures). The thin lines represent the analytic solution obtained by finding the Parsons solution with the same Rossby and Burger numbers (omitting a thin western boundary current).

There is a very good agreement between our solution and BHB's. The outcrop line follows a very similar path. The outcrop intersects the northern boundary at exactly the same gridpoint, and the western boundary slightly further north in our model, than in BHB. We find our maximum layer thickness is 1.89 in the centre of the gyre, and in figure (11) it is 1.90. We note a substantially smaller outcrop area on these numerical solutions compared with the analytic solution. This is consistent with the analytic solutions' higher maximum thickness of 2.36. The layer thickness on the eastern wall ( $h'_e$ ) is 0.55 in the analytic solution and varies between about 0.5 and 0.6 in our model. We note that these numerical solutions have relatively high friction and so layer thickness contours intersect the eastern wall. The close agreement

between our model and that of BHB leads us to believe the model is accurately reproducing the numerical solution.

Figure(12) is a run with twice the inertial length scale twice the Rossby radius and half the frictional length scale of figure(10). The analytic solution depends only on one parameter which Parsons calls  $\lambda$ . In our notation this is  $R_o/\pi B_u$  so the analytic solutions corresponding to the parameters in figures (10) and (12) are the same. In this figure the layer thickness minimum is about  $-2 \times 10^{-3}$  and the maximum is 2.02 times the mean thickness. The analytic solution is again shown in thin lined contours.

The most noticeable differences are in the overshoot. The separation of the jet from the western wall is no longer a smooth right hand turn into the basin. Rather the fluid overshoots the smooth separation latitude, dissipating vorticity (via friction) until it can smoothly plunge south again to rejoin the mostly inertialess separated jet. It is interesting to compare the influence of inertial effects upon this outcropping solution with the inertial but mostly non-divergent solutions of figs (7 and 8). The character of these almost non-divergent solutions is completely altered by the inertial effects, as the northern inertial boundary current is necessary to remove excess relative vorticity.

In the outcropped solutions with small inertia we already have a northern like frictional boundary current (*i.e.* the separated jet) which removes the excess vorticity, not accounted for by the western (also frictional) boundary current. The increased inertial effects do not substantially change the character of the solution since the sink of vorticity is the overshoot which extends the path of parcels heading for the separated jet. Hence it is difficult to see how an 'overspun' inertial solution such as fig(8) can be obtained in single gyre situations where outcropping occurs except through the somewhat artificial mechanism, of the overshoot hitting the northern wall.

In this solution the layer thickness minimum is about  $-2 \times 10^{-3}$  and the maximum is 2.02 times the mean thickness. The analytic solution is again

shown in thin lined contours.

We have been unable to obtain solutions with a significantly higher Rossby number, due to weak non-linear instability in some advection terms. A future paper will examine solutions with significantly higher inertia where the Parsons solution is not valid.

Finally we look at some double gyre results with outcropping. These experiments are in a basin six thousand kilometres square centered at  $45^\circ$  degrees north corresponding to a value of  $\gamma$  of 0.57. The wind forcing is  $\tau_x = -\cos(2\pi y/L)$  and  $\tau_y = 0$ . Typically authors who have looked at single layer double gyre solutions in the ocean have been looking at quasi-geostrophic or barotropic non-divergent solutions with the purpose of studying eddies, or parameterisation (*e.g.* Marshall 1984). Since we have been using a model which does not necessarily have an accurate spin-up (see section 2) we have chosen to look at pure steady states with outcropping.

To verify the effectiveness of our model we first reproduce fig.(2d) of Huang(1986). The parameters are such that the inertial and frictional length scales are 1/129th and 1/33th of the basin respectively, and the Rossby Radius is 1/236th the basin size. Figures (13 and 14) are our model and Huang's results respectively. Clearly these are very similar, they both have maximum thickness of 2.30 and the outcrop lines are almost identical.

Figure (15) shows where the model has been run with sixteen times the Rossby number and sixteen times the Burger number hence exactly the same analytical outcrop line. Again we see the efficient manner in which parcels remove vorticity by extending their path near the separating jet. Although inertial effects are important especially near the mid-basin jet, the majority of the basin is essentially in Sverdrup type linear balance.

## 6 Discussion

In this paper we have built an ocean model based upon the semi-geostrophic equations. We believe this model to be the first balanced model to allow drying up of shallow water layers. It has been found to be both robust in its numerical formulation and versatile in its applications and has been able to reproduce classical results of idealised gyre theory. This balanced model is able to examine solutions where large layer thickness variations and high inertial non-linearity are both included.

Our model uses linear drag dissipation. A shallow water model with gravity waves included would almost certainly need higher (differential) order dissipative forms (such as Laplacian) providing a sink of enstrophy on the grid scale, to aid numerical stability (Sadourny 1975). Indeed we built a vorticity conserving 'B' grid numerical model with flux corrected transport (of layer thickness  $h$ ) and linear drag dissipation. We found that it was able to reproduce the solutions with small Rossby number effectively (*i.e.* fig. 13), but at higher and higher Rossby number it degenerated into grid-scale noise.

We found that a shallow water model was usually quicker computationally than our semi-geostrophic balanced model although we made no great effort to optimise our balanced model. We found that one step of our balanced model using the tridiagonal inverter technique (with two iterations) described in section 2 took approximately twice as long as one step of the shallow water model (on a Cray XMP). Solving the non-constant coefficient elliptic inversion (eq. 39) took about twice as long as the tridiagonal inversion technique.

The time step in a shallow water model was set by the internal gravity wave speed ( $\Delta t < \Delta x / \sqrt{g'h}$ ). The semi-geostrophic model had its time step set either by advection ( $\Delta t < \Delta x / u$ ) or by Kelvin waves ( $\Delta t < f^{-1}$ ). So the balanced model was most cost effective when layers were thick or the Burger number high, and least effective when looking at non-linear solutions, with high advection velocities and weak stratification. The use of a semi-implicit

primitive equation model (Kwizak and Robert 1971, Hurlbert and Thompson 1980) is likely to be quicker than either of the above approaches (see, for example, the timings in Barth *et al.* 1990) since these models require only the solution of a constant coefficient Helmholtz type equation (which can be solved by FFT's when in rectangular domains) rather than the much more expensive non-constant coefficient problems that balanced models more advanced than quasi-geostrophic tend to require. The time step for semi-implicit models is set by advection and  $f^{-1}$  as in our semi-geostrophic model.

It is unlikely that a balanced model (other than quasi-geostrophic ones) will be significantly more efficient than a semi-implicit primitive equation model. The advantages of using a balanced numerical model are likely to come from the lack of gravity waves. Numerical models have sources of gravity waves from non-physical origins, such as coordinate surfaces intersecting topography, poor resolution of bottom topography, poor representation of momentum advection terms, spurious (and/or unrealistic) forcing terms and parameterisations. These spurious gravity waves interact and may significantly corrupt the 'slow' (geostrophic) flow of physical interest. Balanced models may therefore represent physical processes more accurately by omitting the poorly represented gravity waves and just modelling the more interesting 'slow' dynamics.

Our semi-geostrophic model supports a Kelvin wave which may propagate at angular frequencies up to the Coriolis parameter. These Kelvin waves are not gravity waves in any sense, they are geostrophic in both directions in contrast to shallow water and primitive equation Kelvin waves. Kelvin waves are known to be present in other balanced models, where the boundary conditions allow a normal geostrophic velocity at boundaries (Gent and McWilliams 1983). It is important to note that unless these waves are modelled accurately that the spin-up process will be severely altered (Anderson and Gill 1975). In balanced models where the Kelvin wave may propagate at angular frequencies up to the Coriolis parameter then a requirement of spin-up accuracy suggests

a practical limit on the time step of  $f^{-1}$ .

We feel this model to be useful because of its versatility and extendability. With the momentum and continuity equation formulation used here we can easily modify the numerical formulation of each term in the equations, add different parameterisations and add extra equations (such as salinity in the ocean or moisture in the atmosphere).

Further enhancements to the model are envisaged with a wider range of applicability. These include a more robust solution technique involving solving for  $\delta U$  and  $\delta V$  simultaneously, positive definite momentum advection (to remove the weak non-linear instability mentioned in section 3 and 5), a many layer version, coastlines and diabatic forcing. Future papers studying outcropping solutions with large inertial effects are in preparation.

### Acknowledgments

John Marshall participated in many useful discussions throughout this work and his help is gratefully acknowledged. PC was supported by NERC, the UK Meteorological Office and UCAR during this work.

Allen, J.S., J.A. Barth and P.A. Newburger, 1990: On Intermediate Models for Barotropic Continental Shelf and Slope Flow Fields: Part I, Formulation and Comparison of Exact Solutions *J. Phys. Oceanogr.*, **20**, 1017-1042.

Anderson, D.L.T. and A.E. Gill, 1975: Spin-up of a stratified ocean, with applications to upwelling. *Deep Sea Res.*, **22**, 583-596.

Asselin, R., 1972: Frequency Filter for Time Integrations *Mon. Wea. Rev.*, **100**, 487-490.

Arakawa, A., 1972: Design of the UCLA general Circulation Model *Numerical Simulation of Weather and Climate, Dept. of Meteorology, Univ. of Calif., Los Angeles, Tech. Rept. 7*, 116pp.

Barth, J.A., J.S. Allen and P.A. Newburger, 1990: On Intermediate Models for Barotropic Continental Shelf and Slope Flow Fields: Part II, Comparison of Numerical Model Solutions in Doubly-Periodic Domains. *J. Phys. Oceanogr.*, **20**, 1042-1050.

Bleck, R. and D.B. Boudra, 1986: Wind-driven spin-up in eddy-resolving ocean models formulated in isopycnic and isobaric coordinates. *J. Geophys. Res.*, **91C**, 7611-7621.

Bogue, N.M., R.X. Huang and K. Bryan, 1986: Verification experiments with an isopycnal coordinate ocean model *J. Phys. Oceanogr.*, **16**, 985-990.

Boris J.P. and D.L. Book, (1973): Flux-corrected transport, 1. SHASTA, A fluid transport Algorithm that works *J. Comp. Phys.*, **11**, 388-69.

Cloke, P., 1992: Semi-Geostrophic Ocean Modelling *PhD Thesis for the Imperial College of the Univ. of London*, , .

Cullen, M.J.P., 1989a: Implicit Finite Difference Methods for Modelling Discontinuous Atmospheric Flows *J. Comp. Phys.*, **81**, 319-348.

Cullen, M.J.P., 1989b: On the Incorporation of Atmospheric Boundary Layer Effects into a Balanced Model *Quart. J. R. Met. Soc.*, **115**, 1109-1131.

Cullen M.J.P. and R.J. Purser, 1989: Properties of the Lagrangian Semi-geostrophic Equations *J. Atmos. Sci.*, **46**, 2684-2697.

- Eliassen A., 1948: The Quasi-static Equations of Motion with Pressure as Independent Variable. *Geophys. Publ.*, **17(3)**, .
- Gent, P.R. and J.C. McWilliams, 1983: Consistent balanced models in bounded and periodic domains. *Dyn. Atmos. Ocean*, **7**, 67-93.
- Hoskins, B.J., 1975: The geostrophic momentum approximation and the semi-geostrophic equations *J. Atmos. Sci.*, **32**, 233-242.
- Huang, R.X., 1986: Numerical Simulation of Wind-driven Circulation in a Subtropical/Subpolar Basin *J. Phys. Oceanogr.*, **16**, 1636-1650.
- Hurlbert, H.E. and J.D. Thompson, 1980: A numerical study of loop current intrusions and eddy shedding *J. Phys. Oceanogr.*, **10**, 1611-1651.
- Kwizak, M. and A.J. Robert, 1971: A semi-implicit scheme for grid point atmospheric models of the primitive equations. *Mon. Wea. Rev.*, **99**, 32-36.
- Magnusdottir, G. and W.G. Schubert, 1990: The Generalization of Semi-geostrophic Theory to a  $\beta$ -plane. *J. Atmos. Sci.*, **47**, 1714-1720.
- Marshall, J.C., 1984: Eddy-mean flow interaction in a barotropic ocean model *Quart. J. R. Met. Soc.*, **110**, 573-590.
- Marshall, J.C., A.J.G. Nurser and R. Brugge, 1988: On the time-mean flow of Quasi-geostrophic wind-driven gyres. *J. Geophys. Res. (Oceans)*, **93(C12)**, 15427-15436.
- McWilliams, J.C. and P.R. Gent, 1980: Intermediate models of planetary circulations in atmosphere and ocean. *J. Atmos. Sci.*, **37**, 1657-1678.
- McWilliams, J.C., N.J. Norton, P.R. Gent and D.B. Haidvogel, 1990: A Linear Balance Model of Wind-driven Mid-latitude ocean Circulation. *J. Phys. Oceanogr.*, **20**, 1349-1378.
- Parsons, A.T., 1969: A Two-Layer Model of Gulf Stream Separation. *J. Fluid Mech.*, **39**, 511-528.
- Robert, A.J., 1966: The Integration of a Low Order Spectral Form of the Primitive Meteorological Equations *J. Met. Soc. Japan, Ser 2*, **44**, 237-245.
- Salmon, R., 1983: Practical use of Hamilton's Principle *J. Fluid Mech.*,

132, 431-444.

Salmon R., 1985: New Equations for Nearly geostrophic flow. *J.Fluid Mech.*, **153**, 461-477.

Shutts, G.J., 1989: Planetary Semi-Geostrophic Equations Derived from Hamilton's Principle *J. Fluid. Mech.*, **208**, 545-573.

Sadourny R., 1975: The Dynamics of Finite Difference models of the Shallow Water Equations *J.Atmos.Sci.*, **32**, 680-689.

Stommel, H., 1948: The Westward Intensification of Wind-driven ocean currents. *Trans. Amer. Geophys. Union*, **99**, 202-206.

Veronis, G., 1966: Wind-driven Ocean Circulation-Part 2. Numerical Solutions of the non-linear problem. *Deep-Sea Res.*, **13**, 31-55.

Williams G.P., 1969: Numerical integration of the Three-dimensional Navier-Stokes equations for Incompressible flow. *J. Fluid. Mech.*, **37**, 727-750.

Zalesak S.T., 1979: Fully multidimensional flux-corrected transport algorithms for fluids. *J.Comp.Phys*, **31**, 335-362.

$1.0 \times 10^{-1}$	$1.0 \times 10^{-1}$	$1.0 \times 10^{-1}$	10.0
$1.0 \times 10^{-2}$	$1.0 \times 10^{-2}$	$1.0 \times 10^{-2}$	1.0
$1.0 \times 10^{-3}$	$1.0 \times 10^{-3}$	$1.0 \times 10^{-3}$	0.1
$1.0 \times 10^{-4}$	$1.0 \times 10^{-4}$	$1.0 \times 10^{-4}$	0.01

Table 1. Table of parameters for figure 1b.

Figure Numbers	Parameters		
	$R_o$	$B_u$	$\epsilon'$
4,5	$1.0 \times 10^{-6}$	100	$2.0 \times 10^{-2}$
6	$4.0 \times 10^{-4}$	100	$2.0 \times 10^{-2}$
7	$1.0 \times 10^{-3}$	100	$1.0 \times 10^{-2}$
8	$1.0 \times 10^{-3}$	100	$8.0 \times 10^{-3}$
9	$4.0 \times 10^{-4}$	$2.0 \times 10^{-3}$	$2.0 \times 10^{-2}$
10,11	$3.1 \times 10^{-4}$	$1.64 \times 10^{-4}$	$6.0 \times 10^{-2}$
12	$1.23 \times 10^{-3}$	$6.56 \times 10^{-4}$	$3.0 \times 10^{-2}$
13, 14	$6.02 \times 10^{-5}$	$1.79 \times 10^{-5}$	$3.0 \times 10^{-2}$
15	$9.63 \times 10^{-4}$	$2.86 \times 10^{-4}$	$3.0 \times 10^{-2}$

Table 1: Table of parameters for figures 4-15.

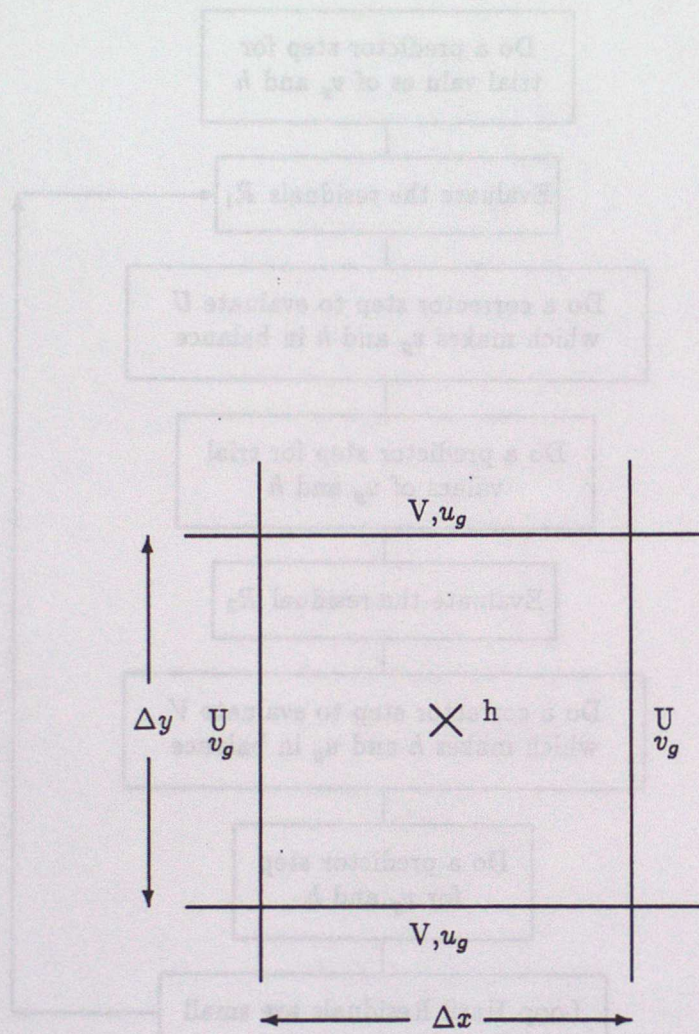


Figure 1: Arrangement of Variables on the Grid

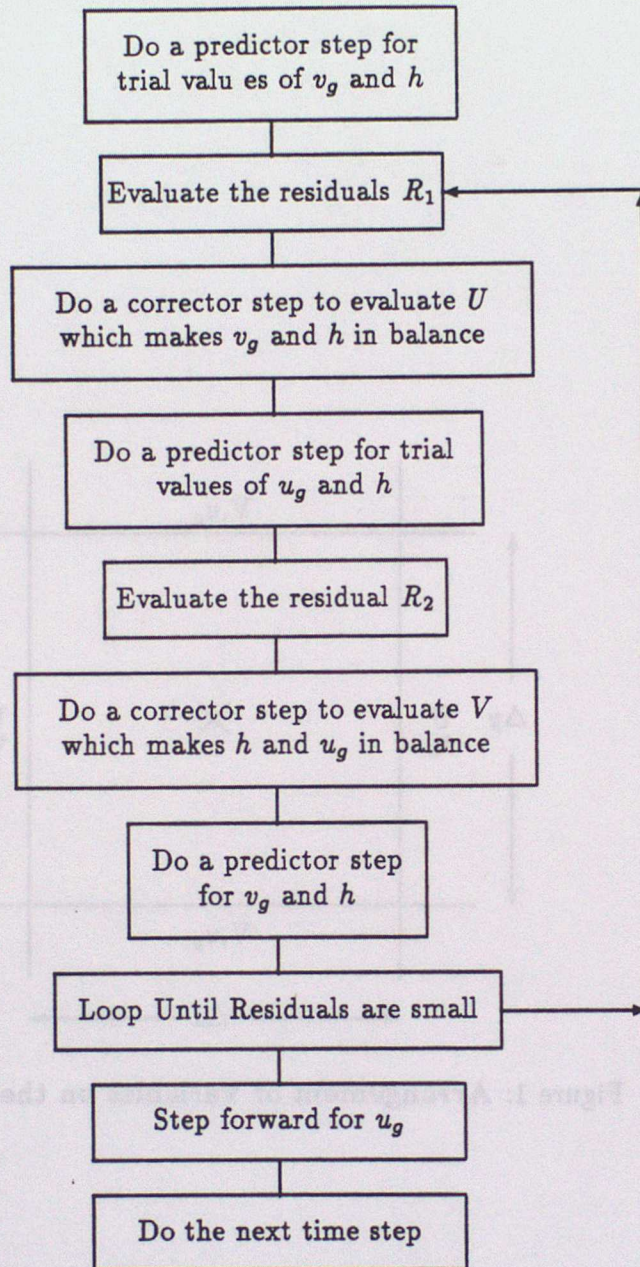


Figure 2: Algorithm for non-outcropping code.

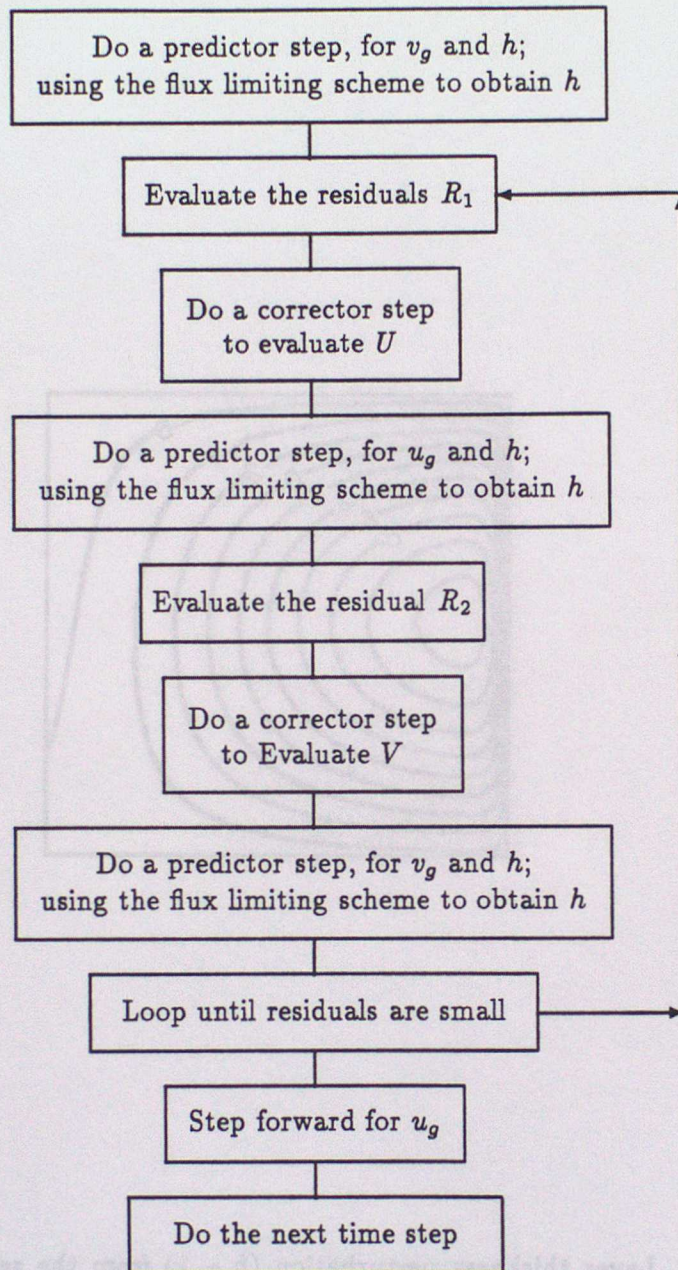


Figure 3: Algorithm for outcropping code.

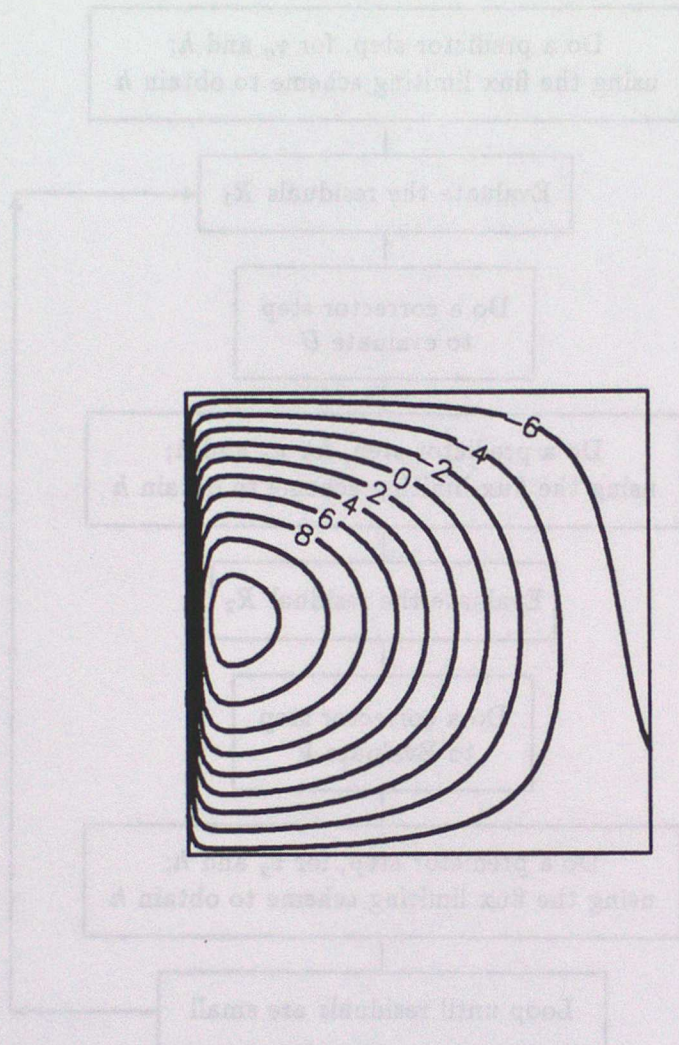


Figure 4: Layer thickness perturbation ( $h - 1$ ) from the semi-geostrophic model. The contour interval is  $2 \times 10^{-9}$ . The solution is reminiscent of the Stommel(1948) solution. Note that the contours intersect the boundary. The parameters are given in table 1

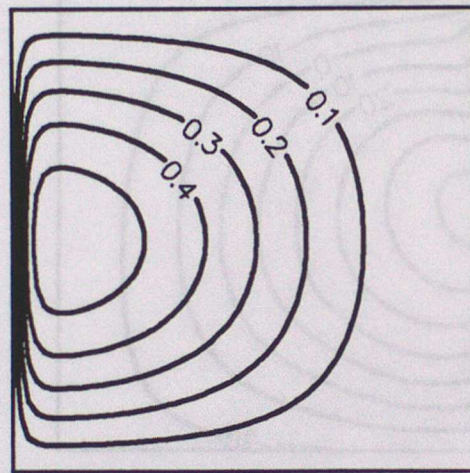


Figure 5: Streamlines from the semi-geostrophic model. Parameters are the same as in fig. 4. Here the streamlines do not intersect the walls. The contour interval is 0.1.

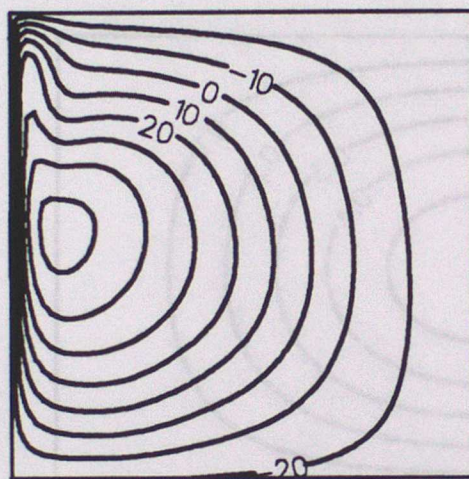


Figure 6: Layer thickness perturbation from our model. With a higher Rossby number ( $4 \times 10^{-4}$ ), hence higher inertia, the purely western boundary current of figures 4 and 5 is replaced with a flow of significant north-south asymmetry. The contour interval is  $1.0 \times 10^{-6}$ .

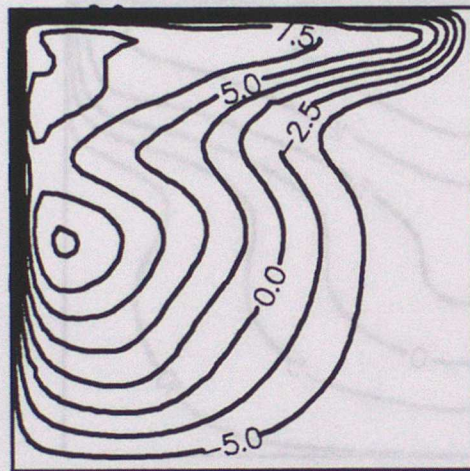


Figure 7: Layer thickness perturbations with yet higher Rossby number ( $1 \times 10^{-3}$ ). The contour interval is  $2.5 \times 10^{-6}$ . The boundary current is both frictional and inertial here.

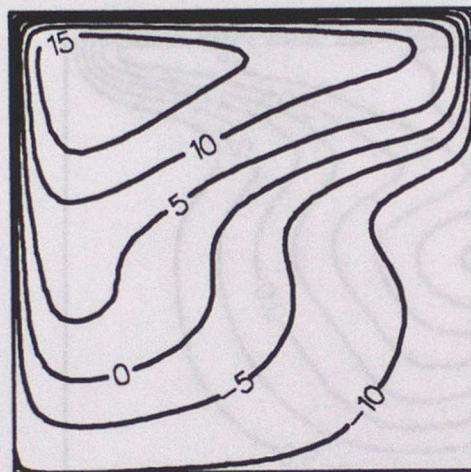


Figure 8: Layer thickness perturbations. Here the friction is decreased relative to figure 7 and the western boundary current has been almost entirely replaced by a northern current. The contours are in units of  $1.0 \times 10^{-6}$ .

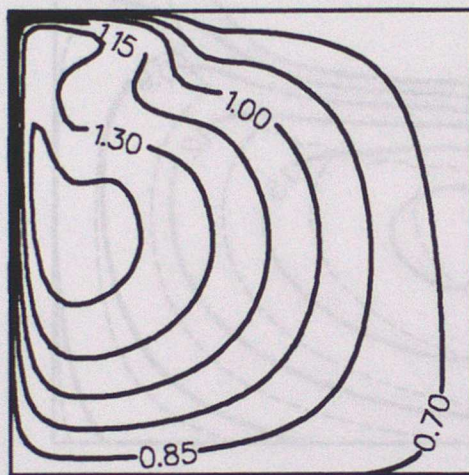


Figure 9: Layer thickness from a run with large thickness variations. The contour interval is 0.15. The parameters (see table 1) are the same as for figure 6 except for the much lower Burger number.

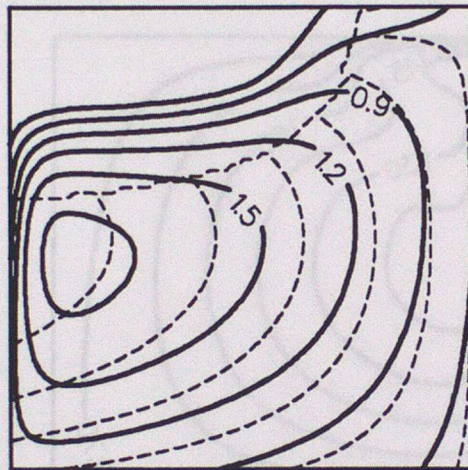


Figure 10: Layer thickness from the outcropping version of our model. The parameters are the same as for fig. 1b of BHB (see also table 1). Continuous lines are from our model, dashed lines are the analytic solution. The contour interval is 0.3.

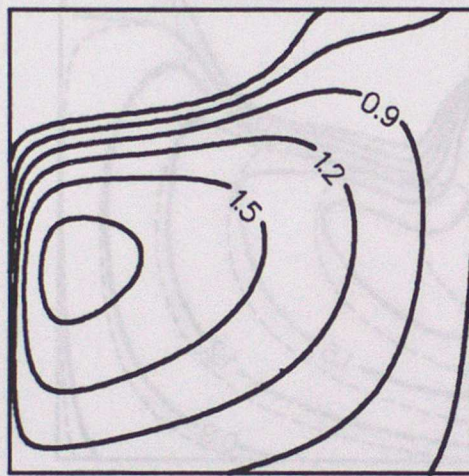


Figure 11: The layer thickness from the model of Bogue et al. (1986,fig. 1b).  
The contour interval is 0.3. Parameters are exactly the same as in figure 10

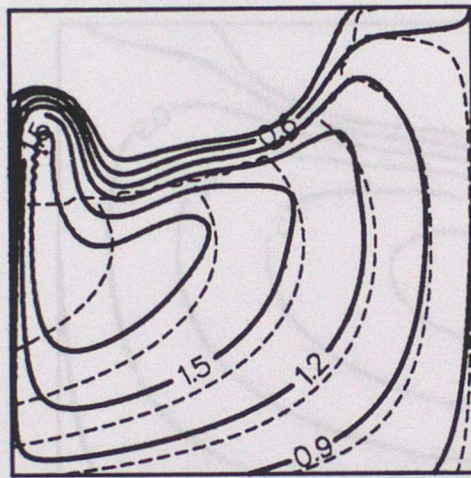


Figure 12: Layer thickness from the outcropping version of our model. Continuous lines are from our model, dashed lines are the analytic solution. Here the inertial length scale is well resolved and the boundary current is clearly overshooting. The contour interval is 0.2 . Linear theory suggest that the solution will be the same as in figures 10 and 11.

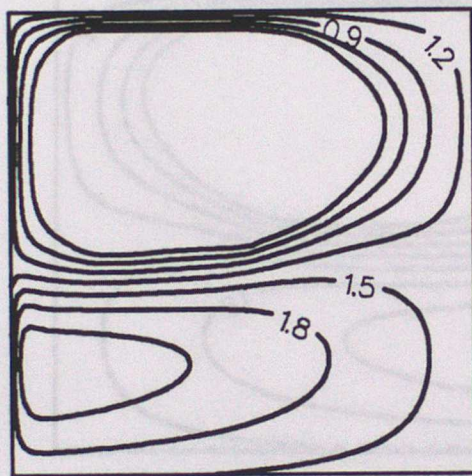


Figure 13: Layer thickness from our model, with the parameters of Huang (1986) fig. 2d. Double gyre forcing is applied. The contour interval is 0.2.

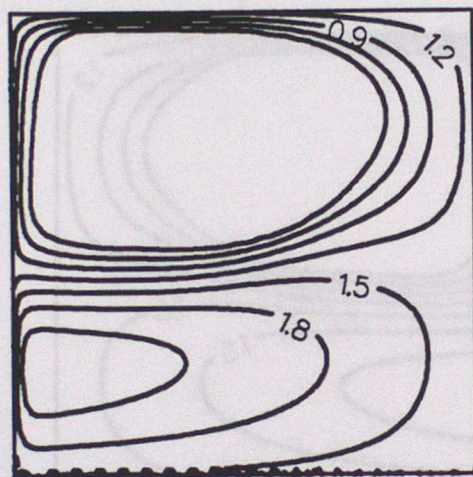


Figure 14: Layer thickness from the model of Huang (1986) parameters as in figure 2d of that paper. The contour interval is 0.2 .

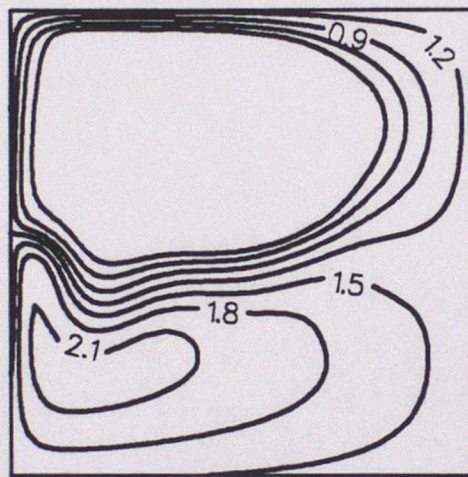


Figure 15: Layer thickness from a double gyre run of our model. We have increased both the Rossby number and the Burger number, but kept the analytical outcrop line constant. The jet is clearly overshooting. The contour interval is 0.2 .